Remote Environmental Monitoring Units: An Autonomous Vehicle for Characterizing Coastal Environments*

MARK A. MOLINE AND SHELLEY M. BLACKWELL

Biological Sciences Department, California Polytechnic State University, San Luis Obispo, California

CHRIS VON ALT, BEN ALLEN, AND THOMAS AUSTIN

Oceanographic Systems Laboratory, Woods Hole Oceanographic Institution, Woods Hole, Massachusetts

JAMES CASE

Marine Science Institute, University of California, Santa Barbara, Santa Barbara, California

NED FORRESTER, ROBERT GOLDSBOROUGH, MIKE PURCELL, AND ROGER STOKEY

Oceanographic Systems Laboratory, Woods Hole Oceanographic Institution, Woods Hole, Massachusetts

(Manuscript received 3 December 2003, in final form 4 August 2004)

ABSTRACT

In oceanography, there has been a growing emphasis on coastal regions, partially because of their inherent complexity, as well as the increasing acknowledgment of anthropogenic impacts. To improve understanding and characterization of coastal dynamics, there has been significant effort devoted to the development of autonomous systems that sample the ocean on relevant scales. Autonomous underwater vehicles (AUVs) are especially well suited for studies of the coastal ocean because they are able to provide near-synoptic spatial observations. These sampling platforms are beginning to transition from the engineering groups that developed and continue to improve them to the science user. With this transition comes novel applications of these vehicles to address new questions in coastal oceanography. Here, the relatively mature Remote Environmental Monitoring Units (REMUS) AUV system is described and assessed. Analysis of data, based on 37 missions and nearly 800 km of in-water operation, shows that the vehicle's navigational error estimates were consistently less than 10 m, and error estimates of mission duration, distance, velocity, and power usage, once the vehicle was properly ballasted, were below 10%. An example of the transition to science is demonstrated in an experiment conducted in 2002 in Monterey Bay, California, where the vehicle was used to quantify critical horizontal length scales of variability. Length scales on the order of tens to hundreds of meters were found for the region within 25 km of the coastline, which has significant implications for designing proper sampling approaches and parameterizing model domains. Results also demonstrate the overall utility of the REMUS vehicle for use by coastal oceanographers.

1. Introduction

Because of the highly dynamic nature of the coastal ocean and the recent acknowledgment of growing anthropogenic impacts, increasing importance is being placed on the development of coastal ocean observatories and autonomous observational platforms that are capable of highly resolved continuous measurements (Schofield et al. 2002). Use of these platforms is essential to an improved understanding and characterization of the physical, chemical, and biological dynamics in the coastal ocean on relevant time and space scales (Dickey 1993; Glenn et al. 2000). Autonomous underwater vehicles (AUVs) are especially well suited for studies of the coastal ocean because they are able to provide continuous spatial and, to some degree, temporal observations. Unlike other platforms, such as moorings and autonomous profilers, which are limited to a fixed lo-

* Center for Coastal Marine Sciences Publication Number 1.

Corresponding author address: Mark A. Moline, Biological Sciences Department, California Polytechnic State University, 1 Grand Ave., San Luis Obispo, CA 93407.
E-mail: mmoline@calpoly.edu

cation, and, in contrast to satellite and airborne sensors, which are often limited to surface measurements, AUVs are capable of characterizing dynamics throughout the water column.

The beginnings of AUV technology date back to the early 1960s at the Applied Physics Laboratory at the University of Washington with the Self-Propelled Underwater Research Vessel (SPURV) (Busby 1977). Significant advances were made in the 1980s at the Marine Systems Engineering Laboratory in New Hampshire where the experimental autonomous vehicle (EAVE) was developed (Blidberg 2001). Since then, a significant number of resources have been devoted to the development of AUV technology and the integration of this technology toward educational, scientific, and military applications (Griffiths 2003). There are generally two classes of AUVs that are being deployed: gliders and propeller-driven AUVs. Autonomous gliders change buoyancy and use wings to convert a fraction of their vertical motion into horizontal velocity. Typical speeds are on the order of 0.7 kt. These systems are designed to patrol the subsurface for weeks to months at a time, surfacing to transmit their data to shore while downloading new instructions at regular intervals. These systems have demonstrated their utility in coastal systems (Davis et al. 2002; Eriksen et al. 2001; Schofield et al. 2003, Sherman et al. 2001; Webb et al. 2001), and, like all classes of AUVs, reveal a tremendous cost savings compared to traditional surface ships. The gliders ability to execute extended missions unattended is of particular importance because it facilitates process studies over temporal and spatial scales that are not achievable by a vessel or many propeller-driven AUVs that require tending by a ship. Because of these extended missions, sensor packages for this type of AUV are often limited by power.

While more limited in duration than autonomous gliders, the propeller-driven AUV systems travel at speeds greater than 2 kt and offer more systematic sampling capabilities with larger payloads and power for sensors. The payload of propeller-driven AUVs provides an excellent opportunity for the oceanographic community to integrate multiple sensors on one vehicle, enabling the simultaneous collection of biological, chemical, and physical data. This capability provides the spatial and temporal context to interpret discrete samples, which have conventionally been the primary data source for our understanding of ecosystem function and response. The simultaneous application of propeller-driven and glider AUVs in observing systems offers the most comprehensive observational approach. Moreover, both types of AUV systems can be directed to sample a particular region or feature adaptively and help to better identify the time and space scales of the dynamic or area of interest (Curtin et. al 1993; Rudnick and Perry 2003).

AUVs have traditionally been operated by teams of engineers involved in or very familiar with the design and engineering aspects of the vehicle (Griffiths 2003). The transition of AUV's from the engineering community into operational tools for use and operation by the science end user has, in the past, been hindered by technological limitations. However, with the rapid advance and maturation in AUV technology in the last 5 yr, this transition is beginning to be realized at a meaningful scale (Blackwell et al. 2002; Brierley et al. 2002; Brierley et al. 2003; Fernandes et al. 2003; Levine and Lueck 1999).

One of the first examples of the transition of AUV technology is the relatively compact propeller-driven Remote Environmental Monitoring Units (REMUS; von Alt et al. 1994; Allen et al. 1997, 2000) developed by the Oceanographic Systems Laboratory at the Woods Hole Oceanographic Institution, and now produced by Hydroid, Inc. (Pocasset, Massachusetts). The REMUS AUV meets a need in the oceanographic community for a small AUV to conduct high-resolution surveys in the nearshore coastal ocean. Currently, there are a total of 56 REMUS vehicles being used in the field. Of these, 48 are used by the United States and international militaries, with the remaining 8 vehicles being operated by academic institutions. The oceanographic applications of these eight vehicles include plume tracking, turbulence characterization, measurements of bioluminescence potential, upwelling/downwelling radiance mapping, and quantification of plankton with an integrated video recorder.

Here we present a comprehensive description of the REMUS vehicle, its principles of operation, and an analysis of the vehicle's performance based on 2 yr of operation on both coasts of the United States in a full range of environmental conditions. A field study demonstrates an application of the vehicle in measuring the inherent complexity in the coastal ocean using variogram analyses (Cressie 1993). Quantification of this complexity is crucial for appropriate sampling design and is a precondition to improved understanding of coastal processes.

2. Vehicle description and performance

The REMUS AUV is a propeller-driven platform that is relatively unique for its small size and durability (Fig. 1). The standard vehicle is 160 cm in length and 19 cm in diameter, it weighs 37 kg, and is hand deployable by two people from a small boat, thus, significantly reducing operating costs. Four lithium-ion batteries

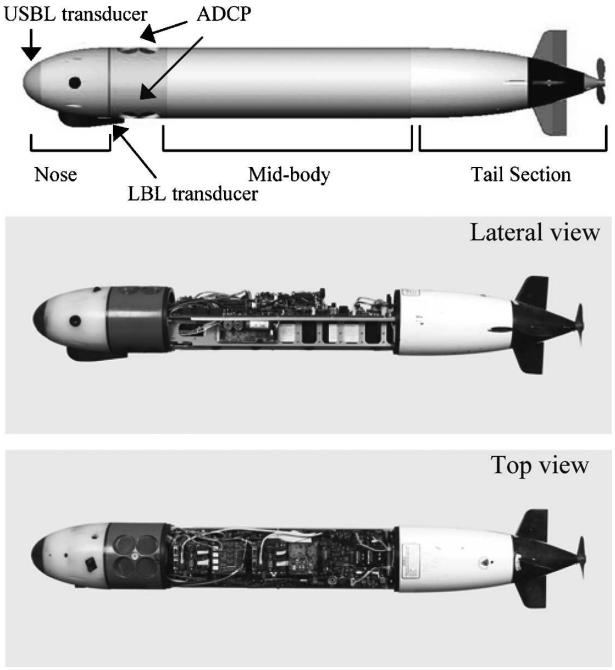

FIG. 1. Schematics of REMUS illustrating the three main sections of the vehicle and internal views of control and power systems.

power the vehicle for maximum mission distances at 3 kt of greater than 80 km. The REMUS has four main sections—a nose section, an RD Instruments acoustic Doppler current profiler (ADCP), a midbody, and a tail section.

The nose section (Fig. 1) includes both the Ultra Short BaseLine (USBL) and Long BaseLine (LBL) acoustic navigation transducers. In addition, this section contains an Ocean Sensors 200 conductivity and temperature sensor. Data are used in real time to calculate the speed of sound for distance calculations during LBL and USBL navigation. Data from a pressure transducer at the bulkhead are also used in real time for the mission navigation to maintain preprogrammed depths. Aft of the nose is the 1200-kHz RD Instruments REMUS Workhorse Navigator ADCP (Fig. 1). This ADCP consists of four upward- and four downward-looking transponder beams. Upward- and downward-looking beam arrays are used to measure current velocity and direction in a range of user-specified depth bins above and below the vehicle. Vehicle velocities and current speed/direction can only be calculated when within range of the bottom. The range limits of the ADCP are between 1 and 20 m above and below the vehicle. The vehicle incorporates the ADCP data to calculate its position in real time, while navigating by compass, and to adjust for currents that may alter the vehicle course. The downward-looking array is also used as an altimeter, allowing for bottom tracking/mapping and a fixed altitude flight.

The midbody of REMUS (Fig. 1) is an airtight chamber, housing the majority of the operational components of the vehicle, including the compass, heading sensors, yaw-rate sensor, and four 26-V/10 A h lithium-ion batteries. The control computer, based on PC-104 technology, is also contained in this section and incorporates a 133-MHz Advance Digital Logic central processing unit (CPU). Leak sensors positioned throughout this section, along with an internal pressure transducer (a vacuum is pulled to ~700 mb), call for a mission-abort routine if triggered. Mission information and all data collected from external sensors are stored on a 1-GB flash disk. Data are downloaded via Ethernet or serial connection using a graphical user interface, which has modules for processing data files, creating HTML reports of the data, and data visualization. The forward tail subsection is a continuation of the midbody airtight compartment, housing the controller circuits for the propulsion and fin motors, the fin motors, and their respective drive assemblies (Fig. 1). The pitch-and-yaw fins are mounted on shafts that extend through the housing of the tail section. The aft tail subsection houses a brushless direct current (DC) propulsion motor. The stator is locked in a small airtight chamber and is separated from the propulsion shaft–mounted magnetic rotor with a thin plastic sleeve. Ceramic bearings and a polyurethane coating on the rotor allow the drive shaft compartment to be flooded and eliminate the need for a shaft seal.

REMUS uses three modes of navigation that are user specified or vehicle determined. Conventionally, the vehicle operates within an array of digital acoustic transponders deployed in the area of study for the duration of a mission. USBL navigation employs a four-channel hydrophone to interrogate the transponders. The hydrophone measures the range and bearing to the transponder from the received signal. Acoustic range and bearing are combined with the vehicle's pitch, roll, and heading information to get an updated absolute fix on the vehicle's position. USBL navigation is utilized for homing in on a single transponder and is more accurate at short ranges. LBL navigation is based on the principles of triangulation. The latitude and longitude of each of the transponders is preprogrammed into the REMUS mission file. The vehicle calculates its position by computing its range to the acoustic transponders with a maximum range of 2.5 km. The majority of LBL navigation error is a result of inaccurate positioning of transponders, with minor error resulting from range measurement uncertainty (~2 m). LBL navigation is

employed for most larger-area missions. During periods between triangulated fixes, or when acoustic fixes are not available, the vehicle navigates in dead reckoning (DR) mode. When operating in this mode, REMUS relies on the compass heading and last known position to navigate to its next programmed waypoint. REMUS incorporates ocean current velocity/direction, vehicle velocity [based on propeller resolution per minute (RPM) and bottom-tracking Doppler signals], and heading information from the vehicle's yaw sensor to estimate its location and navigate accordingly. The DR navigational accuracy depends on oceanic conditions and the error in the vehicle's magnetic compass (~2.3°). To minimize error, each mission begins with a compass calibration, with compensations applied during acoustic navigation.

From 2001 to 2003 the California Polytechnic State University REMUS (A/V *Boomerang I*) completed 37 missions for a total cumulative distance traveled of 766 km. Of the 766 km traveled, 565 km were traveled with the vehicle operating outside the range of the acoustic network. While the successful operation outside of the network effectively increases the operational area and utility of the vehicle, the lack of absolute navigational information based on known coordinate locations makes it difficult to conduct accurate operational analysis. Therefore, the following analyses were conducted on the 201 km of data when the vehicle was within the acoustic network. Navigational error for missions representative of calm estuarine waters (20 July 2001), the moderately calm Pacific Ocean (1 August 2002), and rough coastal seas to 3 m (1 January 2002) in Fig. 2 show that positional error varied little between the three deployments and was less than 3.5 ± 8.5 m for all three missions. The nine missions between 10 and 18 August 2003 show greater navigational error (open squares in Fig. 2) than the previous three. Error for these nine missions is presented only for the first 2.5 km of more than a 40-km overall mission and represents only the part of the mission when the vehicle was within range of the acoustic transponders. The higher variability in navigation during these missions might be attributed to a strong western flow of up to 25 cm s^{-1}. A comparison of the navigational error with and without the USBL nose in place is also presented in Fig. 2. The small difference in navigational error (<2 m) between the mission with the USBL nose on 21 March 2002 and the mission without the USBL nose on 25 March 2002 demonstrates that the vehicles ability to navigate accurately is not compromised by removing the USBL nose and replacing it with the bioluminescence bathyphotometer nosecone.

Table 1 summarizes the vehicle's performance errors

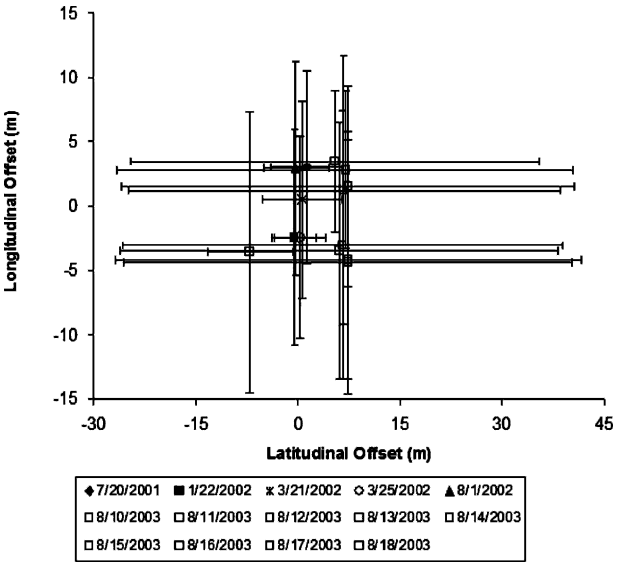

FIG. 2. Average navigational error of REMUS during 14 different missions in a variety of different ocean conditions, ranging from calm estuarine to rough coastal waters. The USBL nose was integrated on 21 Mar 2002 with the comparative mission when the bioluminescence nosecone was in place on 25 Mar 2002.

for a set of operational parameters, including mission duration, distance traveled, power usage, and achievement of predefined velocities for the 201 km of operation within the acoustic network. Operational errors for each of the 37 missions were determined by calculating the percent difference between the predicted or goal parameter value and the actual or achieved value. Percent error was reported rather than the average absolute differences because there were differences in distance and duration for many of the missions, and in order to most accurately represent the vehicles performance. Mission duration, power usage, and vehicle velocity are parameters that the vehicle calculates prior to a mission that depend on the vehicle's propeller calibration coefficient. This coefficient defines the distance traveled per propeller revolution. At the end of each mission the vehicle reports the calibration coefficient for that specific mission based on the total number of propeller revolutions and the distance traveled. This distance is determined using the navigation information from the acoustic transponders and ground tracking information from the ADCP. The updated coefficient is then entered by the user into the vehicle's configuration file and is used to project estimates of the operational parameters for subsequent missions. The ability to redefine this coefficient allows the vehicle to make more accurate predictions of mission duration and power usage and to more successfully achieve predefined velocities.

TABLE 1. Summary of percent error in estimation of REMUS operational parameters, based on 766 km of underway operation from 37 missions. Table includes errors from missions before reballasting to account for bioluminescence nosecone ($n = 19$) and those that were operated after reballasting ($n = 18$).

	Duration	Distance	Velocity	Power usage
		Overall		
Percent error	−5.02 ± 8.8	0.45 ± 6.8	4.7 ± 6.8	−3.7 ± 16.7
Error ranges	−22.0/6.4	−8.4/20.9	−9.5/15.8	−53.0/30.5
		Before ballasting		
Percent error	−8.6 ± 9.1	3.7 ± 6.1	7.4 ± 7.0	−3.4 ± 20.25
Error ranges	−22.0/6.4	−8.4/20.9	−9.5/15.8	−53.0/30.5
		After ballasting		
Percent error	1.7 ± 2.7	−3.8 ± 5.0	−0.02 ± 3.0	−0.2 ± 9.3
Error ranges	−2.3/6.3	−8.3 + −3.8	−2.4/7.1	−9.22/−0.1

During the 37 missions included in this analysis, the vehicle was deployed in environmental conditions ranging from estuary waters that were virtually free of current or swell, to deployments off of the coast of California in swells up to 3 m and currents up to at least 25 cm s^{-1}. Of the 37 missions, only 5 were in calm estuary environments, 2 were approximately 5-km offshore within the Long-Term Ecosystem Observatory (LEO)-15 network of the mid-Atlantic Bight, and the remaining 30 missions were off the coast of central California. During these missions the operational errors were, on average, below 10%. Table 1 also provides a performance analysis before and after the vehicle was reballasted to account for the positive buoyancy of the bioluminescence nosecone, and indicates an improvement in the vehicles ability to estimate duration and power consumption and to achieve a predefined velocity after reballasting.

The aforementioned analysis included four missions with the standard USBL nose in place, whereas the remaining 33 missions had the bioluminescence nose cone attached (see section 3 below). Comparison of the performance parameters from the same ~12 km mission in San Luis Obispo Bay run with and without the USBL nose for navigation show that the percent error differed by less than 3% for each of the operational parameters, and the average navigational offset during the mission with the USBL nose was only slightly better (offset < 1.0 m) than when the USBL nose was replaced with the bioluminescence nosecone (offset $<$ 2.5 m).

In addition to the importance of the vehicle being able to navigate accurately, it is integral to mission planning that accurate estimates of power consumption are made. While Table 1 provides an overall look at the vehicles ability to estimate power consumption, Fig. 3 shows the actual power (watts) consumption as a function of the vehicle's RPM during the 14 missions represented in Fig. 2. The point density distribution in this figure show that for the majority of the time the power estimate is accurately described by the equation

$$\text{power} = (\text{hotel load})(\text{calibration coefficient})\text{RPM}^3. \quad (1)$$

The points that are to the left or above the theoretical curve in black suggest situations in which the vehicle has exceeded the bollard threshold and the prop has momentarily shut down. One possible circumstance in which this would occur is if the vehicle is at the surface and is trying to dive down. The cluster of observations that fall to the right of the curve is most probably a result of noisy data at the operational power load (80 W), because the propeller and brushless motor were not designed to achieve 2000 RPM in the water. In spite of the number of points above and below the curve, the relationship and data density distribution in this figure and the low error in estimating power consumption (Table 1) indicate predictable and consistent power consumption, which is important for longer deployments when using the full capacity of the batteries, as well as for integration of auxiliary instruments.

3. Vehicle sensors

a. Bioluminescence bathyphotometer

A bioluminescence bathyphotometer (BP) was newly designed and developed for integration into the REMUS vehicle's front end (Moline et al. 2000; Blackwell 2002; Herren et al. 2005). The REMUS BP is a modification of the original bioluminescence bathyphotometer design (Herren 2002; Herren et al. 2005) and is made up of three subsections: a nose cone, the light measuring section, and an instrument interface section (Fig. 4). Bioluminescence in the ocean is biologically generated light, which is triggered by a chemical and/or mechanical stimulation (Herring 1978). Although bioluminescence is present in nearly 700 genera, the de-

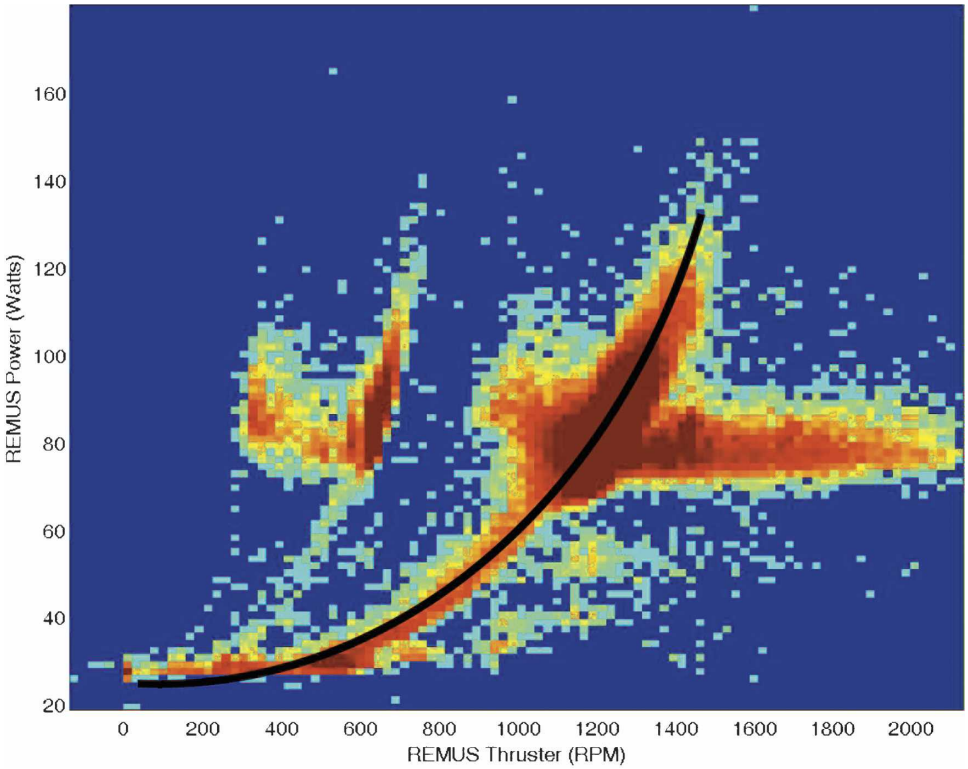

FIG. 3. Point density plot representing the power response as a function of propeller RPM during the 14 missions represented in Fig. 2. Higher densities of observations are represented in red and low densities are in blue.

velopment/application of this sensor was focused on subcentimeter planktonic organisms. To prevent premature stimulation of bioluminescence by the moving vehicle, a newly designed nose incorporates the water intake of the BP in the tip of the nose, and replaces the conventional USBL section. Two light-baffling turns serve to minimize ambient light contamination. A centrifugal-type impeller pump drives the water into an enclosed 500-mL chamber in the BP section, where a light-baffled photomultiplier tube (PMT; Hamatsu H5783) measures stimulated bioluminescence between 300 and 650 nm. The inside of the chamber is coated with a 0.075-mm flat white coating to maximize the amount of stimulated light measured by the PMT. As the water passes into the detection chamber, the impeller pump creates turbulent flow, which mechanically stimulates bioluminescence. The flow rate through the chamber is dependent upon the rotation rate of the impeller rotor. This rate is adjusted to achieve residence times of 1.2–1.4 s, or flow rates of approximately 400 mL s^{-1}. A flowmeter monitors pumping rates using a magnet and a Hall effect sensor to generate a period signal, which is converted to an analog signal of flow rate. The flow rates are measured as the water passes from the detection chamber to exhaust outlets that lead to the exterior of the vehicle. No significant ram effect from the vehicle itself is evident in the flow-rate data.

b. Auxilliary sensors

Unique to the A/V *Boomerang I* is a section between the BP and the vehicle's bulkhead incorporating the Seapoint fluorometer and optical backscatter sensors, the Ocean Sensors 200 CTD sensor, and the LBL transducer. Both the fluorometer and optical backscatter sensor project beyond the vehicle contour for maximal flushing. The CTD sensor is housed in a streamline-imbedded indentation along the top of the vehicle. Flushing is maximized over the CTD sensor with a Bernoulli-principled plate partially covering the top of the sensor well. The fluorometer has an excitation wavelength of 470 nm and detects fluorescence of chlorophyll a at 685 nm. The sensing volume of the fluorometer is ~340 mm^3. Sensitivity can be set to one of four gains and the minimum detection limit is 0.02 μg Chl a L^{-1}. The optical backscatter sensor can also be set to one of four gains and measures backscattered light at 880 nm. The backscattered light is measured between 15° and 150°; therefore, only the volume of water within

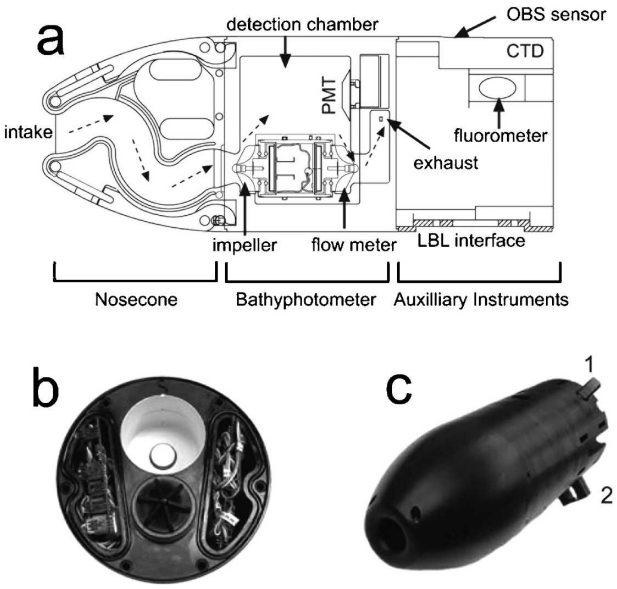

FIG. 4. (a) Schematic of the REMUS bioluminescence bathyphotometer. Water flow is indicated by hashed arrows; turbulent flow within detection chamber is generated by the impeller. Two exhaust openings are located on either side of the instrument. The interface section incorporates the fluorometer, optical backscatter sensor (on opposite side of figure), CTD sensor, and LBL transducer. (b) Cross section illustrating the lateral housing for the electrical components: (bottom center) impeller, and (top center) light detection chamber. (c) Exterior of REMUS bathyphotometer showing the 1) optical backscatter sensor and 2) fluorometer.

5 cm of the sensor windows is actually measured. This volume is determined by the angle of light emission from the LED and the scatterance angles that are measured by the photodiode detector. All sensors can be individually accessed through a serial debugger via the vehicle's graphical user interface (GUI). Data from the fluorometer, optical backscatter sensor, BP, and CTD are recorded at user-defined frequencies (2–12 Hz) and are stored on board the vehicle. In addition to these sensors and the ADCP (see above), the REMUS has also incorporated a number of other sensors that are specific to user applications, such as the 600- or 900-kHz MSTL AUV model side-scan sonar, and an externally mounted Sontek acoustic Doppler velocimeter and shear probe (Levine and Lueck 1999).

4. Field application

a. Deployment approach

In a study conducted in August 2002, the A/V *Boomerang I* was deployed as part of a larger effort in Monterey Bay to examine the impacts of offshore and bay circulation patterns on the nearshore distributions of biological communities. Vehicle missions were run at night (0600–1400 UTC), because bioluminescence was one of the main parameters being measured, and to avoid any possible effects of solar quenching of the fluorescence (Falkowski and Raven 1997). During these deployments, the vehicle's traditional LBL acoustic navigation near shore was supplemented with DR to increase the operational range of the vehicle in order to survey a larger area of Monterey Bay. The vehicle was programmed to first run a series of four 500-m lines spaced 20 m apart along the same 180° heading as the 20-km transect line (Fig. 5). These initial four lines allowed the vehicle, while still in range of the acoustic transponders, to correct for any compass error before setting off on the 20-km offshore transect. On four missions between 21 and 26 August 2002, the vehicle navigated 20 km offshore to the M1 mooring in the center of Monterey Bay (Chavez et al. 1997), undulating between 3 and 40 m. The vehicle then made a 180° turn, back toward shore, remaining at a constant depth of 20 m. Four transponders were set up along 4 km of coastline to work as an acoustic net on the return trip. Upon nearing the acoustic range of the transponders, the vehicle would reestablish communications with the transponders, obtain a position offset, and adjust its position accordingly to complete the mission at the starting location. The length of the acoustic net was designed to provide sufficient coverage in the event that the vehicle had incurred the maximal position offset (~1.6 km) that was predicted based on compass error and the dis-

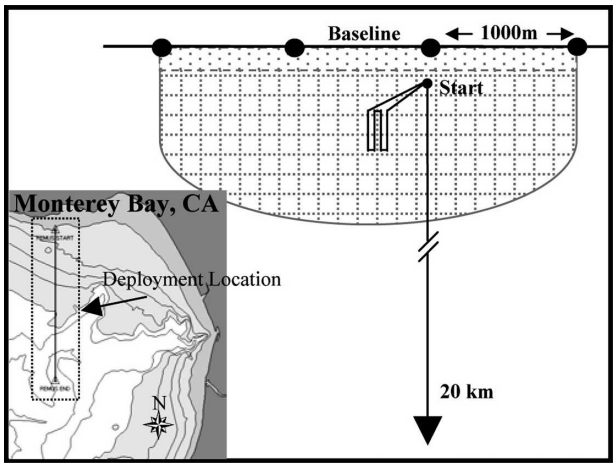

FIG. 5. Map of the deployment location in Monterey Bay, CA. The schematic demonstrates geometric configuration between transponders (black circles) and vehicle survey area (solid line). Grid region delineates functional communication limits between vehicle and transponders (2500 m; beyond this region the vehicle dead reckons). Dotted region located nearest to the baseline is 212 m wide and denotes the limit of effective vehicle triangulation.

tance traveled. During each of the four missions, the vehicle was tracked with a ranging transducer deployed from the R/V *Paragon*. The ranges to the vehicle and the boat's position were recorded approximately every 2 km. Positions were recorded to calculate the maximum distance/time deviations of the A/V *Boomerang I* from the predefined mission course. Although a vessel was used in these deployments as a means to assess along- and cross-track errors, the A/V *Boomerang I* is traditionally deployed by swimmers and conducts missions without the use of a tending vessel. This is important to mention because few propeller-driven AUVs have demonstrated true autonomous operation.

b. Data collection and statistical analysis

Data were collected at 2 Hz and the vehicle was traveling at 1.7 m s^{-1}, yielding a horizontal data resolution of 0.85 m. In any situation where the objective is to produce a synoptic map of spatial variability, the Doppler-shift effect resulting from sequential sampling of a moving instrument can make it difficult to distinguish between spatial and temporal variability. During this study the vehicle was traveling more than 1.5 orders of magnitude faster than the fastest measured current speeds and for the statistics described here the Doppler-shift effect is assumed to be negligible.

To identify length scales of variability inherent in the Monterey Bay region, observational data (density, optical backscatter, fluorescence, and bioluminescence) were first fit to a generalized additive model (GAM) with independent, locally weighted smooth distance and depth terms. GAM was selected because it can be used to fit nonnormal data. Furthermore, by using an additive model versus a linear model the data are fit using nonparametric functions estimated from the data using smoothing operations. This was accomplished using a loess smoothing function with the span equal to 0.1, which is equivalent to smoothing the data using a 2-km running mean. Each parameter was modeled separately using depth and distance offshore as predictor variables. To remove global spatial trends in the data (i.e., a progressive increase in fluorescence near shore) the residuals of the GAM were used to model an exponential variogram (Cressie 1993). Because the objective was to identify horizontal length scales of variability, a look angle of 11.25° was applied to the variogram analysis. As an objective means of identifying minimum length scales, the range of the fitted variogram defined minimum length scales. The range of the fitted variogram is the distance at which the variogram function reaches the asymptote and becomes a random function, where the variability in the function is attributed to white noise. Ranges were identified separately for the water masses above and below the dominant pycnocline of 1025.3 kg m^{-3}.

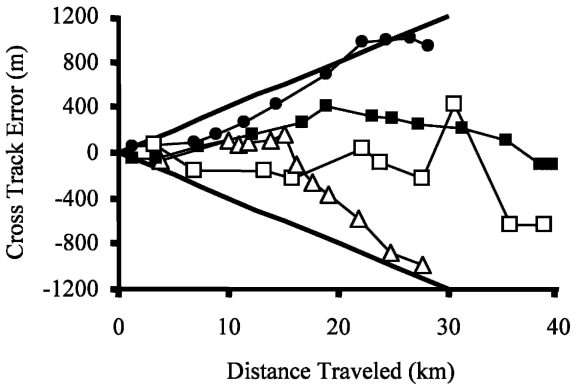

FIG. 6. Maximum cross-track error (CTE) incurred by REMUS as a function of the distance traveled along the transect on four different nights: 21 (open squares), 23 (open triangles), 25 (filled squares), and 26 (filled circles) Aug. Westerly CTE is denoted by negative distances and easterly CTE is denoted by positive distances. Solid black lines represent maximum predicted error defined by the 2.3° compass error.

c. Results

Tracking of REMUS enabled the examination of the vehicle's incurred cross- and along-track error as a function of distance along the primary transect line. Although the cross-track error is the combination of both compass deviation and the local current directions/velocities around the vehicle, mission results demonstrated the ability of the vehicle to operate in DR mode even with additional sensors impacting the streamline of the vehicle. On each of the first three nights the incurred cross-track error did not exceed the maximum predicted by the predefined vehicle error (Fig. 6; 2.3° compass error or 40 m per 1-km distance traveled). The only occasion on which the vehicle incurred more error than that predicted was during the mission beginning on 25 August at 22.2 km along the transect. At this point, the vehicle had incurred a maximum of 972 m of cross-track error, compared to the predicted threshold of 880 m. By the end of the mission, however, the cross-track error was only 941.8 m, 185 m less than that predicted for the total distance traveled (28.2 km).

The vehicle showed significantly greater along-track error than cross-track error. This is not unexpected given that the vehicle was out of range of the bottom for bottom tracking with the ADCP, and beyond the acoustic network for more than 80% of each mission. Cross-track error could be somewhat minimized by heading adjustments made according to the vehicle compass, however, only the propeller calibration coef-

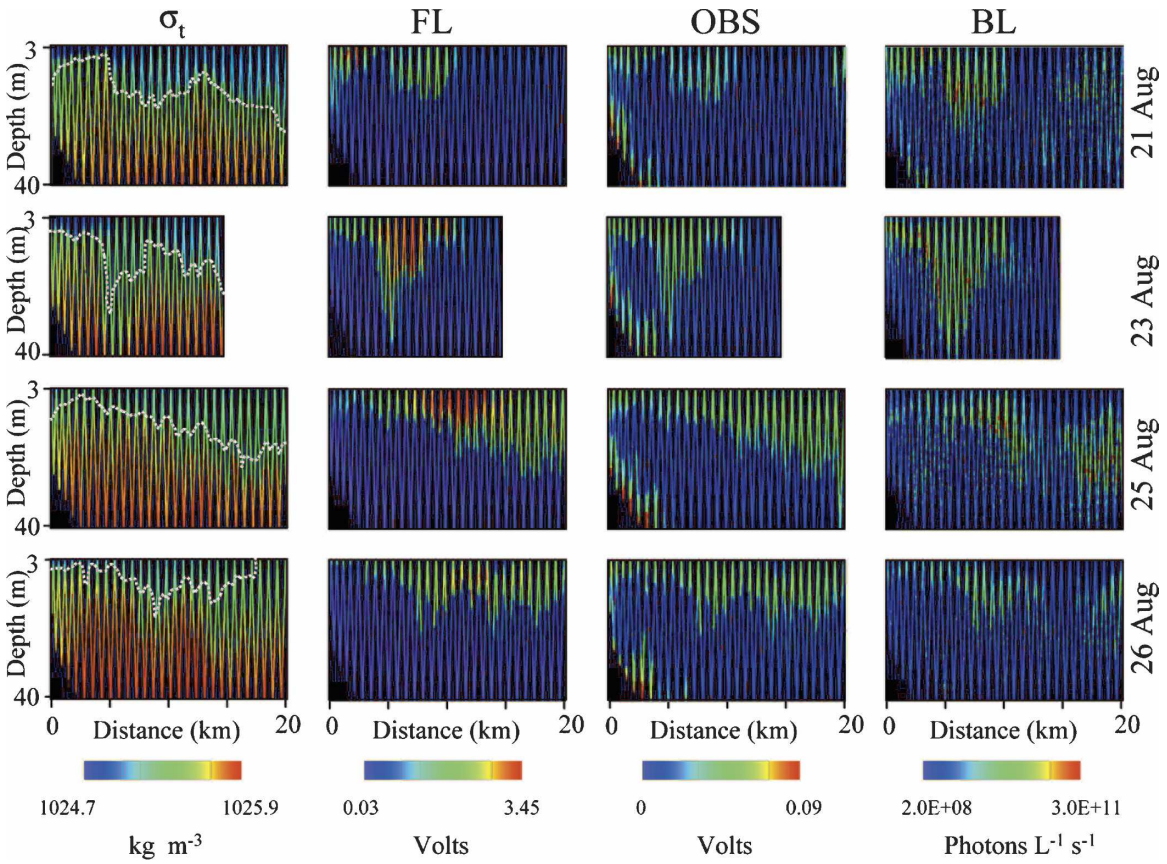

FIG. 7. Measured density (σ_t), fluorescence (FL), optical backscatter (OBS), and bioluminescence (BL) collected by the REMUS AUV along the transect shown in Fig. 3 from north to south. Rows represent nightly transects measured between 21 and 26 Aug 2000. White contour lines show the maximum density gradient (1025.3 kg m^{-3}) and indicate where the water column was separated for statistical analyses.

ficient (centimeters moved forward per revolution) was available for achieving the predefined velocity. A fourfold increase in the along-track error was observed between the first mission and the following three missions, which is suggestive of a change in current patterns after 21 August. Nearshore north/south current measurements (data not shown) show a shift in current direction and velocity from a weak southward flow (1.8 cm s^{-1}) to a flow fluctuating between 20 (north) and 10 (south) cm s^{-1}, which may explain the increase in along-track error after 21 August.

The patterns of distribution of density, fluorescence, optical backscatter, and bioluminescence differed between each of the four missions (Fig. 7), illustrating the highly variable nature of the coastal ocean over time scales of days. There was a general shallowing of the pycnocline inshore with an overall cooling of the surface waters offshore from ~14.5° to 12.5°C. A nearshore phytoplankton bloom appeared to intensify and deepened in spatial extent through 22 August along the transect line. Currents measured near shore (data not shown) suggest the majority of the phytoplankton biomass advected to the west over the course of the week sampling period. The vertical distribution of the bloom corresponded closely to the pycnocline and the fluorescence maximum was consistently above the pycnocline. Optical backscatter showed a very similar dynamic to fluorescence with the exception of high optical backscatter found near the bottom of the first 5 km of the transect; indicative of a benthic nepheloid layer and/or particle resuspension. This was particularly evident on 22, 24, and 25 August where high optical backscatter did not correspond to the fluorescence or bioluminescence signals. Bioluminescence distributions onshore were correlated in part with fluorescence above the pycnocline and also were advected offshore during the sampling period. Noncoherent bioluminescence distributions were found farther offshore (20 August) and deeper (22, 24, and 25 August) than peak fluorescence distributions and suggest heterotrophic sources of bioluminescence.

Quantification of horizontal length scales of variabil-

TABLE 2. Horizontal length scales calculated for density (σ_t), optical backscatter (OBS), fluorescence (FL), and bioluminescence (BL). Values are shown in meters for the upper and lower layers of the water column separated by the maximum density gradient as shown in Fig. 7.

Date	σ_t	OBS	FL	BL
Upper layer				
21 Aug	48	209	367	201
23 Aug	69	89	99	55
25 Aug	48	176	153	103
26 Aug	28	124	64	98
Lower layer				
21 Aug	204	155	274	166
23 Aug	154	126	218	76
25 Aug	193	230	181	69
26 Aug	230	189	184	75

ity using variogram analyses was used as a means to identify the complexity present in the survey area and to better define appropriate sampling approaches. Table 2 summarizes the scales of variability for each of the measured parameters and highlights the dynamic nature of coastal regions. Length scales identified for density above the pycnocline ranged from 28 to 69 m; those below the pycnocline were significantly larger, ranging from 154 to 230 m. Likewise, length scales for fluorescence and optical backscatter, with the exception of 20 August, are consistently larger below the pycnocline, ranging from 126 to 248 m. In contrast, bioluminescence data from 3 of the 4 days (20, 24, and 25 August) showed smaller length scales below the pycnocline.

5. Discussion

With more than 750 km of data presented, this study demonstrates the REMUS as an operationally dependable autonomous underwater platform. The adaptable payload capacity and ease of use makes the vehicle an effective tool for the general oceanographic community. Quantification of navigational error over 12 missions, 3 of which represented differing environmental conditions, and a time series of nine consecutive daily deployments showed that when the vehicle was operating within the acoustic network it was within 6.3 ± 2.2 m of its intended location (Fig. 2). Quantification of the vehicle's accuracy when in dead-reckoning mode showed that the navigational error incurred did not exceed that predicted by the inherent compass error of 2.3°, except on one occasion. This result, in effect, extends the operational area of the vehicle, and enables surveys of near-surface waters (0–100 m) over extreme depths, such as the Monterey Canyon. General performance statistics from the 37 missions show that the vehicle achieved its preprogrammed velocities, accomplished missions within estimated durations, and traveled distances with less than a 10% margin of error from what was predefined. This is especially promising given the environmental operating conditions of the 37 missions, ranging from >3 m swells in 3-m water depth in the Pacific to calm conditions in the Atlantic. In addition, seven missions conducted from the California Polytechnic State University pier in Avila Beach, representing over 100 km of data, are some of the first demonstrations of complete autonomy in a propeller-driven AUV, whereby the vehicle was deployed and retrieved without ever putting a vessel in the water.

Horizontal length scales that are identified using variogram analysis help to define the minimal sampling resolutions required for adequate characterization of the inherent variability in oceanographic parameters. The relatively short length scales identified during this study in Monterey Bay underscore the need for platforms capable of high-resolution sampling in the nearshore ocean. While previous studies from the mid-Atlantic Bight (Chang et al. 2002) and Massachusetts and Cape Cod Bays (Yu et al. 2002) showed that spatial decorrelation length scales of chlorophyll fluorescence, identified using the autocorrelation function, ranged from 3 to 9 km and from 1.6 to 2.0 km, respectively, this study identified scales of variability that are one to two orders of magnitude less, ranging from tens to hundreds of meters (Table 2). Although the studies occurred in different oceans with different oceanographic conditions, this difference in scales raises the question of statistical and methodological approaches. As a direct comparison data from 20 to 26 August 2002 in the current study were analyzed according to methods described in Chang et al. (2002) and Yu et al. (2002). The decorrelation length scales identified were of the same magnitude (100–500 m) as those identified by variogram analysis (Table 2). Bissett et al (2004) also arrived at length scales ranging from tens to hundreds of meters within 10 km of shore a new approach, whereby the standard deviation of an increasingly larger region of interest (ROI) is estimated. The size of the ROI at which the standard deviation increased was defined as the optimal ground sampling distance (analogous to a decorrelation length scale). The three statistical techniques presented here have all quantified scales from tens to hundreds of meters emphasizing the need for higher-resolution observations in coastal waters. While there are some aspects of variogram analysis and the autocorrelation function that need refinement, such as the development of an objective means of determining the smoothing parameters used to detrend the data,

these approaches help to further our understanding of coastal ocean dynamics.

In this study, the smaller scales of variability in fluorescence and optical backscatter above the pycnocline suggest that there is more complexity within the mixed layer, where there is an increased influence of external factors such as light, surface heating, and wind mixing and currents, and differential phytoplankton growth rates and community structure (Li 2002). The pattern of increased length scales in bioluminescence below the pycnocline was consistent with the observation that the majority of bioluminescence at these depths was attributed to zooplankton. Zooplankton have been observed to be more intermittently distributed than phytoplankton and, therefore, require increased sampling resolution in order to characterize their distributions and spatial variability (Folt and Burns 1999). Because bioluminescence can be used as a proxy measure for biomass (Lapota 1998), these results have implications for ecosystem modeling efforts and for the sampling approaches used to validate ecosystem models. These data and analyses also underscore the importance of providing a spatial perspective when attempting to interpret discrete samples, data from profiles, and data from fixed assets, such as moorings.

Acknowledgments. We thank a number of undergraduates from California Polytechnic State University for help with AUV deployments. We also appreciate the logistical support network provided by Oscar Schofield and Scott Glenn in the mid-Atlantic Bight, and Steven Haddock, Hans Thomas, and the crew of the R/V *Paragon* in Monterey Bay. This work was supported by the Office of Naval Research (N00014-00-1-0570 and N00014-03-1-0341 to M. Moline).

REFERENCES

Allen, B., R. Stokey, T. Austin, N. Forrester, R. Goldsborough, M. Purcell, and C. von Alt, 1997: REMUS: A small, low cost AUV; system description, field trials and performance results. *IEEE Oceans Conf. '97*, Halifax, NS, Canada, IEEE, 994–1000.

——, W. Vorus, and T. Prestero, 2000: Propulsion system performance enhancements on REMUS AUV's. *MTS/IEEE Oceans Conf. 2000*, Providence, RI, MTS–IEEE, 1869–1873.

Bissett, W. P., R. A. Arnone, C. O. Davis, T. D. Dickey, D. Dye, D. D. R. Kohler, and R. W. Gould, 2004: From meters to kilometers. *Oceanography*, **17,** 32–42.

Blackwell, S. M., 2002: A new platform for studying bioluminescence in the coastal ocean. M.S. thesis, Biological Sciences Department, California Polytechnic State University, 101 pp.

——, J. Case, S. M. Glenn, J. Kohut, M. A. Moline, M. Purcell, O. Schofield, and C. von Alt, 2002: A new AUV platform for studying near shore bioluminescence structure. *Bioluminescence and Chemiluminescence Progress and Current Applications*, L. J. Kricka and P. E. Stanley, Eds., World Scientific, 197–200.

Blidberg, D. R., 2001: The development of autonomous underwater vehicles (AUVs): A brief summary. *IEEE Int. Conf. on Robotics and Automation '01*, Seoul, South Korea, IEEE, 12.

Brierley, A. S., and Coauthors, 2002: Antarctic krill under sea ice: Elevated abundance in a narrow band just south of ice edge. *Science,* **295,** 1890–1892.

——, and Coauthors, 2003: An investigation of avoidance by Antarctic krill of RRS James Clark Ross using the Autosub-2 Autonomous Underwater Vehicle. *Fish. Res.,* **60,** 569–576.

Busby, R. F., 1977: Unmanned submersibles. *Submersibles and Their Use in Ocenaography and Ocean Engineering*, R. A. Geyer, Ed., Elsevier, 23–59.

Chang, G. C., T. D. Dickey, O. Schofield, A. D. Weidemann, E. Boss, W. S. Pegau, M. A. Moline, and S. M. Glenn, 2002: Nearshore physical processes and bio-optical properties in the New York Bight. *J. Geophys. Res.,* **107,** 3133, doi:10.1029/2001JC001018.

Chavez, F. P., J. T. Pennington, R. Herlien, H. Jannasch, G. Thurmond, and G. E. Friederich, 1997: Moorings and drifters for real-time interdisciplinary oceanography. *J. Atmos. Oceanic Technol.,* **14,** 1199–1211.

Cressie, N. A. C., 1993: *Statistics for Spatial Data*. J. Wiley & Sons, 928 pp.

Curtin, T., J. Bellingham, J. Catipovic, and D. Webb, 1993: Autonomous oceanographic sampling networks. *Oceanography,* **6,** 86–94.

Davis, R. E., C. C. Eriksen, and C. P. Jones, 2002: Autonomous buoyancy-driven underwater gliders. *Technology and Applications of Autonomous Underwater Vehicles*, G. Griffiths, Ed., Taylor and Francis, 37–58.

Dickey, T., 1993: Sensors and systems for sampling/measuring ocean processes extending over nine orders of magnitude. *Sea Technol.,* **34,** 47–55.

Eriksen, C. C., T. J. Osse, R. D. Light, T. Wen, T. W. Lehman, P. L. Sabin, J. W. Ballard, and A. M. Chiodi, 2001: Seaglider: A long range autonomous underwater vehicle for oceanographic research. *IEEE J. Oceanic Eng.,* **26,** 424–436.

Falkowski, P. G., and J. Raven, 1997: *Aquatic Photosynthesis*. Blackwell, 375 pp.

Fernandes, P. G., P. Stevenson, A. S. Brierley, F. Armstrong, and E. J. Simmonds, 2003: Autonomous underwater vehicles: Future platforms for fisheries acoustics. *ICES J. Mar. Sci.,* **60,** 684–691.

Folt, C. L., and C. W. Burns, 1999: Biological drivers of zooplankton patchiness. *Trends Ecol. Evol.,* **14,** 300–305.

Glenn, S. M., T. D. Dickey, B. Parker, and W. C. Boiourt, 2000: Long-term real-time coastal observation networks. *Oceanography,* **13,** 24–34.

Griffiths, G., 2003: *Technologies and Applications of Autonomous Underwater Vehicles.* Taylor and Francis, 342 pp.

Herren, C. H., 2002: The distribution of bioluminescent plankton: Association with marine snow and thin layers. Ph.D. thesis, Marine Science Institute, University of California, Santa Barbara, 166 pp.

——, S. H. Haddock, C. Johnson, M. A. Moline, C. M. Orrico, and J. F. Case, 2005: A multi-platform bathyphotometer for fine scale, coastal bioluminescence research. *Limnol. Oceanogr. Methods,* **3,** 247–262.

Herring, P. J., 1978: *Bioluminescence in Action*. Academic Press, 215 pp.

Lapota, D., 1998: Long term and seasonal changes in dinoflagellate bioluminscence in the Southern California Bight. Ph.D. thesis, Marine Science Institute, University of California, Santa Barbara, 215 pp.

Levine, E. R., and R. G. Lueck, 1999: Turbulence measurements with an autonomous underwater vehicle. *J. Atmos. Oceanic Technol.*, **16,** 1533–1544.

Li, W. K., 2002: Macroecological patterns of phytoplankton in northwestern North Atlantic Ocean. *Nature,* **419,** 154–157.

Moline, M. A., E. K. Heine, J. F. Case, C. M. Herren, and O. Schofield, 2000: Spatial and temporal variability of bioluminescence potential in coastal regions. *Proceedings of the 11th International Symposium on Bioluminescence and Chemiluminescence*, J. F. Case et al., Eds., World Scientific, 123–126.

Rudnick, D. L., and M. J. Perry, 2003: ALPS: Autonomous and Lagrangian Platforms and Sensors. ALPS Workshop Rep., 64 pp. [Available online at http://www.geo-prose.com/ALPS.]

Schofield, O., T. Bergmann, W. P. Bisset, J. F. Grassle, D. B. Haidvogel, J. Kohut, M. A. Moline, and S. M. Glenn, 2002: The long-term ecosystem observatory. *J. Oceanic Eng.,* **27,** 146–154.

——, W. P. Bisset, T. K. Frazer, D. Iglesias-Rodriguez, M. A. Moline, and S. M. Glenn, 2003: Development of regional coastal ocean observatories and the potential benefits to marine sanctuaries. *Mar. Technol. Soc.,* **37,** 54–67.

Sherman, J., R. E. Davis, W. B. Owens, and J. Valdes, 2001: The autonomous underwater glider "Spray." *IEEE J. Oceanic Eng.,* **26,** 437–446.

von Alt, C., B. Allen, T. Austin, and R. Stokey, 1994: Remote environmental measuring units. *IEEE Oceanic Society Newsletter*, Vol. 29, No. 1, 9–14.

Webb, D. C., P. J. Simonetti, and C. P. Jones, 2001: Slocum: An underwater glider propelled by environmental energy. *IEEE J. Oceanic Eng.,* **26,** 447–452.

Yu, X., T. Dickey, J. Bellingham, D. Manov, and K. Streitlien, 2002: The application of autonomous underwater vehicles for interdisciplinary measurements in Massachusetts and Cape Cod Bays. *Contin. Shelf Res.*, **22,** 2225–2245.